A conserved protein network controls assembly of the outer kinetochore and its ability to sustain tension

Iain M. Cheeseman,[1,3] Sherry Niessen,[2] Scott Anderson,[2] Francie Hyndman,[1] John R. Yates III,[2] Karen Oegema,[1] and Arshad Desai[1,4]

[1]Ludwig Institute for Cancer Research, La Jolla, California 92093, USA; [2]Department of Cell Biology, The Scripps Research Institute, La Jolla, California 92037, USA

Kinetochores play an essential role in chromosome segregation by forming dynamic connections with spindle microtubules. Here, we identify a set of 10 copurifying kinetochore proteins from *Caenorhabditis elegans*, seven of which were previously uncharacterized. Using in vivo assays to monitor chromosome segregation, kinetochore assembly, and the mechanical stability of chromosome–microtubule attachments, we show that this copurifying protein network plays a central role at the kinetochore–microtubule interface. In addition, our analysis suggests that the network is comprised of three groups of proteins that contribute in distinct ways to this interface: KNL proteins act after the assembly of centromeric chromatin to generate the core of the microtubule-binding interface, MIS proteins control the rate and extent of formation of this interface, and NDC proteins are necessary to sustain tension during interactions with spindle microtubules. We also purify a similar set of associated proteins from human cells that includes four novel proteins and has recognizable homologs from each functional class. Thus, this protein network is a conserved constituent of the outer kinetochore, and the functions defined by our analysis in *C. elegans* are likely to be widely relevant.

[*Keywords*: Mitosis; centromere; microtubule; spindle; *Caenorhabditis elegans*]

Supplemental material is available at http://www.genesdev.org.

Received June 25, 2004; revised version accepted August 3, 2004.

Accurate chromosome segregation in eukaryotes is achieved by dynamic interactions between chromosomes and spindle microtubules. As cells enter mitosis, each of the two sister chromatids that comprise a mitotic chromosome assembles a kinetochore, a specialized organelle that links the chromatids to spindle microtubules (for review, see Cleveland et al. 2003). Forces generated by kinetochores and the spindle drive chromosome alignment and, following dissolution of chromatid cohesion, segregation to opposite sides of the cell. The action of these forces is coupled to dynamic changes in the length of kinetochore-bound microtubule polymers. The magnitude of the forces acting on kinetochores is significantly greater than that required to generate chromosome movements (Nicklas 1988). The excess force is most likely used to generate tension across bipolar attachments that can be used to select correctly oriented chromosomes and prevent aneuploidy (for review, see Cheeseman and Desai 2004). Thus, kinetochores form attachments to spindle microtubules that couple dynamic polymer length changes to chromosome movement while sustaining significant forces.

To understand how kinetochores generate a microtubule-binding interface with these properties, we are examining kinetochore function in the early *Caenorhabditis elegans* embryo. In contrast to the localized centromeres of vertebrates, *C. elegans* chromosomes are holocentric with diffuse kinetochores that form along their entire length. Despite this difference in chromosome architecture, the structure and molecular composition of *C. elegans* kinetochores is similar to that of other metazoans (Maddox et al. 2004). The *C. elegans* embryo is uniquely suited to the functional analysis of essential kinetochore components because RNA interference (RNAi) can be used to generate oocytes almost completely depleted of a targeted protein. Following fertilization, the consequences of removing a specific kinetochore protein can be assessed during the first mitotic division that occurs in its absence.

Initial work in *C. elegans* has focused primarily on conserved kinetochore proteins including CENP-A^{HCP-3}

Corresponding authors.
[3]E-MAIL icheeseman@ucsd.edu; FAX (858) 534-7750.
[4]E-MAIL abdesai@ucsd.edu; FAX (858) 534-7750.
Article and publication are at http://www.genesdev.org/cgi/doi/10.1101/gad.1234104.

and CENP-C^{HCP-4} (Buchwitz et al. 1999; Moore and Roth 2001; Oegema et al. 2001; Desai et al. 2003), which are thought to establish the specialized centromeric chromatin and direct kinetochore assembly. Depletion of CENP-A^{HCP-3} and CENP-C^{HCP-4} results in a distinctive "kinetochore-null" (KNL) phenotype characterized by failure to distribute chromosomes on a metaphase plate, absence of anaphase chromosome segregation, and failure of all tested kinetochore components to localize to chromosomes (Oegema et al. 2001; Desai et al. 2003). Depleted embryos also display rapid and premature separation of their spindle poles. During the first division in wild-type embryos, strong astral forces pull on the poles to asymmetrically position the spindle prior to cytokinesis (Grill et al. 2001). These pulling forces are normally resisted by the combination of stable attachment of sister kinetochores to microtubules anchored in opposite spindle poles and cohesion between sister chromatids, generating tension in the spindle. In CENP-A^{HCP-3} and CENP-C^{HCP-4} depleted embryos, the absence of kinetochore–microtubule interactions capable of sustaining this tension results in premature pole separation. Thus, the natural forces exerted on spindle poles in the one-cell *C. elegans* embryo can be exploited to provide an indirect readout for the mechanical stability of the kinetochore–microtubule interface (Oegema et al. 2001; Desai et al. 2003).

Using the cytological signatures associated with the "kinetochore-null" (KNL) phenotype to assess results from an RNAi-based screen, we previously identified KNL-1, a kinetochore protein that functions downstream of CENP-A^{HCP-3} and CENP-C^{HCP-4} to generate a functional microtubule-binding interface (Desai et al. 2003). Here, we extend this approach to identify KNL-3, whose depletion also results in a KNL phenotype. Mass spectrometric analysis of KNL-1- and KNL-3-interacting proteins identified a network of 10 copurifying proteins including three established kinetochore components and seven previously uncharacterized *C. elegans* proteins, all of which localize to kinetochores throughout mitosis. Analysis of the phenotypes associated with depletion of each component and of the relationships between them during kinetochore assembly indicate that this network plays a central role in the assembly and function of the microtubule-binding interface. We also identify a similar protein network in human cells indicating that it represents a conserved constituent of the outer kinetochore and that the conclusions from the functional analysis in *C. elegans* are likely to be widely relevant.

Results

Identification of KNL-3, a novel protein whose depletion results in a 'kinetochore-null' phenotype

During an ongoing RNAi-based functional genomic screen in *C. elegans*, we identified a previously uncharacterized gene, T10B5.6, whose inhibition results in a "kinetochore-null" (KNL) phenotype characterized by a failure of chromosome segregation and rapid premature separation of spindle poles. To date, inhibition of only three other proteins results in this specific phenotype: CENP-A^{HCP-3} and CENP-C^{HCP-4}, two widely conserved proteins that form the specialized chromatin at the base of the kinetochore (Oegema et al. 2001), and KNL-1, a recently identified protein that functions after CENP-A and CENP-C to build the outer kinetochore (Desai et al. 2003). Based on the observed phenotype, we named the T10B5.6 gene *knl-3*. Time-lapse sequences visualizing both chromosomes (GFP–histone H2B; Fig. 1A, arrow) and spindle poles (GFP–γ-tubulin; Fig. 1A, arrowheads) clearly illustrate the similar consequences of depleting KNL-3 and KNL-1 (Fig. 1A; Supplementary Videos 1–3). In addition to the qualitative similarity of the depletion phenotypes, the kinetics of spindle pole separation, which are an indirect readout of the mechanical stability of the kinetochore–microtubule interface in the one-cell stage *C. elegans* embryo (Oegema et al. 2001; Desai et al. 2003), are quantitatively identical between KNL-1- and KNL-3-depleted embryos, but distinct from wild type (Fig. 1B).

Consistent with the phenotypic analysis, endogenous KNL-3 and a GFP–KNL-3 fusion protein expressed in the germ line by stable integration both localized to the diffuse mitotic kinetochores of *C. elegans* (Fig. 1C; Supplementary Video 10). KNL-3 staining overlaps with the bona fide kinetochore component CENP-C^{HCP-4} (Fig. 1D). Like CENP-C^{HCP-4} and KNL-1, KNL-3 is first detected on chromosomes during prophase and persists on chromosomes until the end of mitosis. Kinetochore targeting of KNL-3 requires CENP-C^{HCP-4}, but not vice versa, as was found previously for KNL-1 (Fig. 1D; Desai et al. 2003). Thus, KNL-3 is the fourth protein whose depletion results in a kinetochore-null phenotype, and, similar to KNL-1, it performs an essential function downstream of CENP-A^{HCP-3} and CENP-C^{HCP-4} at the mitotic *C. elegans* kinetochore.

Biochemical identification of KNL-1- and KNL-3-interacting proteins

The similar depletion phenotypes and localization requirements of KNL-1 and KNL-3 prompted us to test whether these proteins physically associate. We began by immunoprecipitating KNL-1 and KNL-3 from whole worm extracts using affinity-purified antibodies (Fig. 2A). Anti-GST (glutathione S-transferase) antibodies were used as a control. Immunoprecipitates (IPs) were eluted with 8 M urea, and mass spectrometry was performed on the entire eluate. This approach contrasts with previous Western blotting and sequencing of individual gel bands from KNL-1 IPs (Desai et al. 2003), which indicated that KNL-1 associated with CENP-C^{HCP-4}, NDC-80, and Nuf2^{HIM-10}.

The sensitivity of the mass spectrometry, use of polyclonal antibodies, and a single-step enrichment protocol resulted in the identification of a large number of proteins in the IPs (54 in anti-KNL-1, 83 in anti-KNL-3, and 24 in control using a 5% sequence coverage cutoff). De-

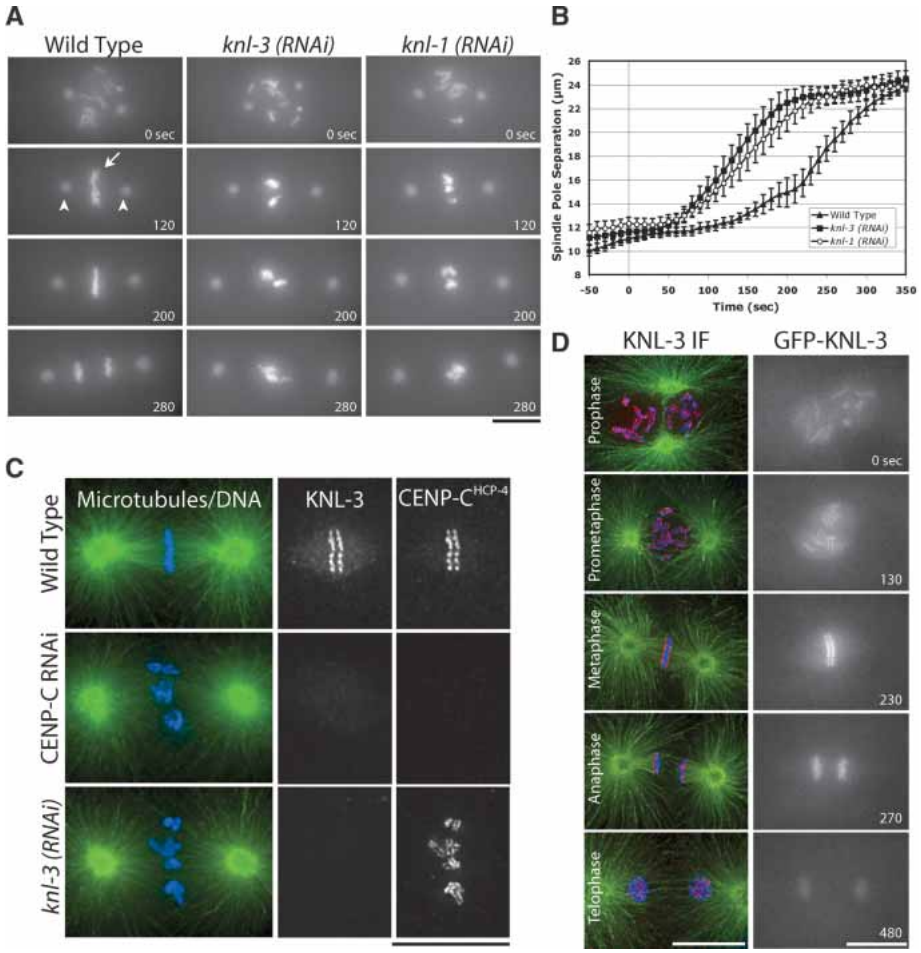

Figure 1. KNL-3 is a kinetochore protein whose depletion results in a kinetochore-null phenotype. (*A*) KNL-3- and KNL-1-depleted embryos exhibit a similar chromosome segregation defect. Selected images from time-lapse sequences of wild-type, KNL-3-depleted, and KNL-1-depleted embryos are shown. Embryos are from a strain coexpressing GFP–histone H2B to mark the chromosomes (arrow) and GFP–γ-tubulin to visualize spindle poles (arrowheads). Time, in seconds after nuclear envelope breakdown (NEBD), is indicated on the *lower right* of each panel. Identical phenotypes were observed in 18 KNL-3-depleted embryos. (*B*) KNL-3- and KNL-1-depleted embryos exhibit quantitatively identical premature spindle pole separation. The kinetics of spindle pole separation are plotted for wild-type (n = 15), KNL-3-depleted (n = 18), and KNL-1-depleted (n = 14) embryos. All sequences were time-aligned with respect to NEBD (0 sec), and the average spindle pole separation was calculated for each time point. Error bars represent the S.E.M. with a confidence interval of 0.95. (*C*) KNL-3 localizes to the kinetochore throughout mitosis. (*Left* column) Immunofluorescence images obtained using affinity-purified antibodies. Microtubules are shown in green, DNA in blue, and KNL-3 in red. (*Right* column) Selected images from a time-lapse sequence of an embryo stably expressing GFP–KNL-3. (*D*) KNL-3 functions downstream from CENP-C^{HCP-4} in the kinetochore assembly hierarchy. Directly labeled affinity-purified antibodies were used to analyze KNL-3 and CENP-C^{HCP-4} localization in wild-type, KNL-3-depleted, and CENP-C^{HCP-4}-depleted embryos. Bars, 10 µm.

spite this complexity, a clear association was observed between KNL-1 and KNL-3, as each was present in the reciprocal IP, but not in the control (Fig. 2C). Therefore, we reasoned that polypeptides found in both KNL-1 and KNL-3 IPs, but not in the control, were likely to be bona fide interacting proteins. These criteria defined a set of 11 proteins: KNL-1, KNL-3, CENP-C^{HCP-4}, NDC-80, Nuf2^{HIM-10}, and the products of the uncharacterized genes Y47G6A.24, R13F6.1, F26F4.13, F26H11.1, Y92C3B.1, and C34B2.2 (Fig. 2C). Because these novel proteins were identified by their physical interaction with KNL-1 and KNL-3, with the exception of Y47G6A.24 (named *mis-12*; see below), we named their corresponding genes *kbp-1* to *kbp-5* for KNL Binding Protein (Fig. 2C). Using RNAi, we found that, except for KBP-5, all of these interacting proteins are required for embryonic viability (Fig. 2C).

Tandem affinity purification supports the identification of a network of 10 interacting proteins

To more rigorously test whether the proteins identified above associate in vivo, we developed a two-step purification procedure based on the tandem affinity purification (TAP) tag (Rigaut et al. 1999). We generated integrated strains stably expressing fusion proteins tagged at

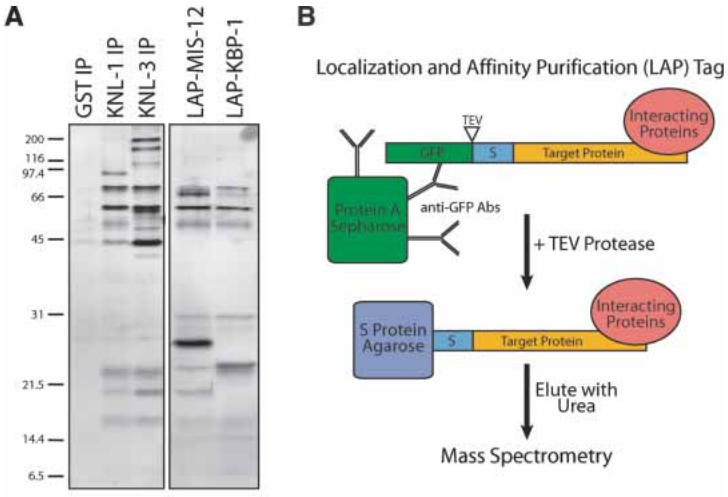

C

Gene Number	Gene Name	% Sequence Coverage KNL-1 (IP)	KNL-3 (IP)	MIS-12 (LAP)	KBP-1 (LAP)	CENP-C^{HCP-4} (IP)	Embryonic Lethality	Size (kDa)
T03F1.9	*hcp-4*	18.9	21.5			*	EMB	97.4
C02F5.1	*knl-1*	*	53.7	16.9	44.9	8.1	EMB	113.2
T10B5.6	*knl-3*	53.9	10.2	25.4	62.7	9.3	EMB	38.4
W01B6.9	*ndc-80*	33.2	39.2	33.4	61.0	5.4	EMB	68.9
R12B2.4	*him-10*	46.7	46.1	32.9	61.2	27.1	EMB	56.7
F26H11.1	*kbp-3*	31.3	30.6		49.0		EMB	15.9
Y47G6A.24	*mis-12*	36.0	26.3	36.0	43.4	20.2	EMB	20.2
R13F6.1	*kbp-1*	36.9	43.6	19.5	49.3		EMB	17.3
F26F4.13	*kbp-2*	49.2	46.0	22.6	71.8		EMB	14.3
Y92C3B.1	*kbp-4*	46.4	29.9	40.2	73.2		EMB	11.5
C34B2.2	*kbp-5*	37.8	36.3	22.2	56.3	21.5	WT	15.7
Total Polypeptides:		54	83	10	11	41		

Figure 2. Purification of KNL-1- and KNL-3-interacting proteins from worm extracts. (*A*) Proteins isolated from worm extracts were fractionated on 14% polyacrylamide gels and visualized by silver staining. (*Left* panel) Immunoprecipitations with antibodies to GST (as a control), KNL-1, or KNL-3. (*Right* panel) LAP-tag purifications of MIS-12 and KBP-1. (*B*) Diagram describing the Localization and Affinity Purification (LAP) tag and the tandem affinity purification scheme. (*C*) Mass spectrometric analysis of the purifications shown in *A* indicating the percent sequence coverage obtained for the indicated proteins. For this analysis, the entire eluate was analyzed (not specific bands). KNL-1, KNL-3, and CENP-C^{HCP-4} are either weakly present or missing in their corresponding immunoprecipitates (indicated by an *) because the 8-M urea elution does not efficiently dissociate antibody–antigen complexes. Therefore, their presence was confirmed using a more stringent secondary elution and Western blotting (data not shown; also see Desai et al. 2003). For IPs, only proteins present in both KNL-1 and KNL-3 IPs, but not in controls, are listed. The predicted molecular mass of each protein as well as the consequence of its depletion on embryonic viability are indicated. EMB refers to >95% embryonic lethality, whereas WT refers to no effect on embryo viability.

their N termini with GFP followed by a TEV protease cleavage site and the S peptide domain that binds to S protein (Fig. 2B). Because this tag allows visualization of a protein's localization and its affinity purification, we refer to it as the Localization and Affinity Purification (LAP) tag. We performed affinity purifications from strains stably expressing LAP fusions with two of the novel proteins identified above (Fig. 2A). Importantly, both fusions localize identically to the endogenous untagged proteins (see Fig. 3). Mass spectrometric analysis revealed that the eluates contain 10 of the 11 proteins from the list obtained by comparison of KNL-1 and KNL-3 IPs (Fig. 2C). In contrast to the IPs, only one apparent contaminant polypeptide (the heat-shock protein HSP-1) was present in the eluates.

Thus, our biochemical analysis defines a group of 10 closely interacting proteins. These proteins also interact more weakly with CENP-C^{HCP-4}, which is the only protein present in both KNL-1 and KNL-3 IPs, but not in the more stringent LAP purifications. Immunoprecipitation of CENP-C^{HCP-4} identified six of the 10 KNL-1/3 interacting proteins, including both KNL-1 and KNL-3, although the sequence coverage is very low (Fig. 2C). Therefore, this group of 10 associated proteins likely interacts closely with the chromatin-proximal domain of the kinetochore established by CENP-A^{HCP-3} and CENP-C^{HCP-4}.

All KNL-1/3-interacting proteins localize to kinetochores

Four of the 10 interacting proteins that we identified (KNL-1, KNL-3, NDC-80, and Nuf2^{HIM-10}) localize to kinetochores throughout mitosis (Fig. 1; Howe et al. 2001; Desai et al. 2003). To examine the localization of the six previously uncharacterized proteins, we first generated affinity-purified polyclonal antibodies against KBP-1, KBP-2, KBP-3, and KBP-4. Immunofluorescence using these antibodies revealed that all four proteins begin to localize to chromosomes during prophase and persist on chromosomes until the end of mitosis. From prometaphase through metaphase, they are visible as paired lines on opposite faces of condensed chromosomes (Fig. 3A). These localizations were specific, because depletion of each protein by RNAi eliminated/severely reduced the corresponding signal (Fig. 3A). To monitor to localization of KBP-1, KBP-3, and KBP-4, we also generated strains stably expressing LAP fusions. Live analysis of embryos from these strains confirmed the kinetochore localization and timing of recruitment that we inferred from analysis of fixed embryos (Fig. 3B; Supplementary Videos). For two of the proteins, MIS-12 and KBP-5, we were unable to obtain antibodies. However, we were able to generate integrated strains expressing LAP fusions that localized to kinetochores with recruitment kinetics

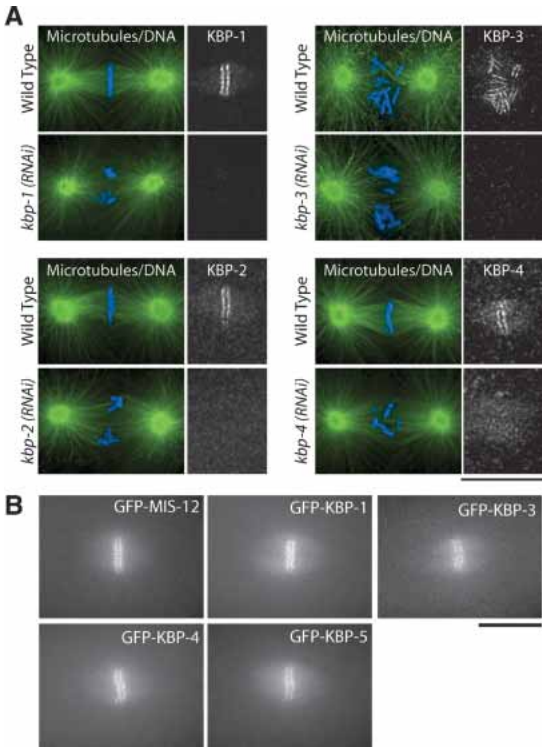

Figure 3. Novel KNL-1/3-interacting proteins localize to kinetochores. (*A*) Immunofluorescence showing localization of endogenous KBP-1, KBP-2, Spc25^{KBP-3}, and KBP-4 to kinetochores using affinity-purified antibodies. Microtubules are shown in green and DNA in blue. Similar stage embryos following RNAi are shown to demonstrate that the observed localization is specific. (*B*) Still images showing localization of LAP-tagged (GFP) fusion proteins for MIS-12, KBP-1, Spc25^{KBP-3}, KBP-4, and KBP-5 during metaphase. Bars, 10 μm.

identical to those observed for KBP-1, KBP-3, and KBP-4 (Fig. 3B; Supplementary Videos). The localization timing that we observed for the six new proteins is also identical to that of KNL-1, KNL-3, NDC-80, and Nuf2^{HIM-10} (Fig. 1; Desai et al. 2003). Thus, all 10 KNL-1/3-interacting proteins localize to kinetochores with a similar temporal profile, consistent with the idea that they function together.

Sequence conservation of KNL-1/3-associated kinetochore proteins

The majority of the new KNL-interacting proteins isolated by our biochemical analysis have clear homologs in *Caenorhabditis briggsae*, a related nematode. In addition, two of these proteins have identifiable homologs outside of nematodes. The first is the product of the Y47G6A.24 gene, which we named MIS-12 based on weak homology to the Mis12 family of kinetochore proteins (Goshima et al. 2003). Pairwise alignments also demonstrated that the protein encoded by *kbp-3*/F26H11.1 shows similarity to the Spc25 family of kinetochore proteins (data not shown). Spc25 associates with Ndc80/HEC and Nuf2, two widely conserved kinetochore components (Janke et al. 2001; Wigge and Kilmartin 2001). Based on the sequence homology, the physical interaction with NDC-80 and Nuf2^{HIM-10}, and the phenotypic analysis described below, we refer to the KBP-3 protein as Spc25^{KBP-3}.

Although KNL-1 was previously reported to lack homologs outside of nematodes (Desai et al. 2003), it shares primary sequence features with the recently identified yeast kinetochore protein Spc105p (J. Kilmartin, pers. comm.). Both KNL-1 and fungal Spc105p contain a series of N-terminal repeats of the amino acid sequence M[E/D][I/L][S/T] and a C-terminal coiled-coil domain (Fig. 4A; also see Desai et al. 2003; Nekrasov et al. 2003). Remarkably, using three M[E/D][I/L][S/T] repeats as an input motif to search the nonredundant protein database using the program Seedtop (available from NCBI; ftp://ftp.ncbi.nlm.nih.gov/blast/executables/LATEST-BLAST), we specifically identified the fungal Spc105s, nematode KNL-1s, and a single human protein, AF15q14. AF15q14 exhibits weak primary sequence homology to Spc105p and KNL-1 and also has a C-terminal coiled-coil domain. All members of this new protein family have an [S/G]ILK and an RRVSF motif at their N termini (Fig. 4A). Thus, the group of 10 associated proteins that copurify with KNL-1 and KNL-3 includes five recognizably conserved proteins: MIS-12, NDC-80, Nuf2^{HIM-10}, Spc25^{KBP-3}, and KNL-1.

Purification of human Mis12 identifies a similar network of interacting proteins

To test whether AF15q14 is the human homolog of KNL-1 and whether humans have a set of interacting proteins orthologous to the network of KNL-1/3-associated proteins that we defined in *C. elegans*, we generated a clonal human cell line stably expressing LAP–hMis12. This fusion protein localizes to human kinetochores, as expected from prior work (Fig. 4B; Goshima et al. 2003). Strikingly, mass spectrometric analysis of the eluates following purification of this fusion protein from human cell extracts (Fig. 4C) identified a set of 10 proteins with significant similarity to the KNL-1/3-interacting proteins from *C. elegans* (Fig. 4D). In addition to hMis12, all four subunits of the human Ndc80 complex (hNdc80/HEC, hNuf2, hSpc24, and hSpc25; Bharadwaj et al. 2004; McCleland et al. 2004) and the predicted KNL-1 homolog AF15q14 were present. The set of hMis12-associated proteins also includes Zwint, which was identified in a two-hybrid screen with the widely conserved metazoan kinetochore protein ZW10 and localizes to human kinetochores throughout mitosis (Starr et al. 2000), as well as three uncharacterized proteins (DC31, Q9H410, and PMF1). To determine whether DC31, Q9H410, PMF1, and AF15q14 represent bona fide kinetochore components, we fused them to YFP and transiently expressed them in human cells. As shown in Figure 4E, each of these fusion proteins localized to paired punctate foci in metaphase tissue culture cells

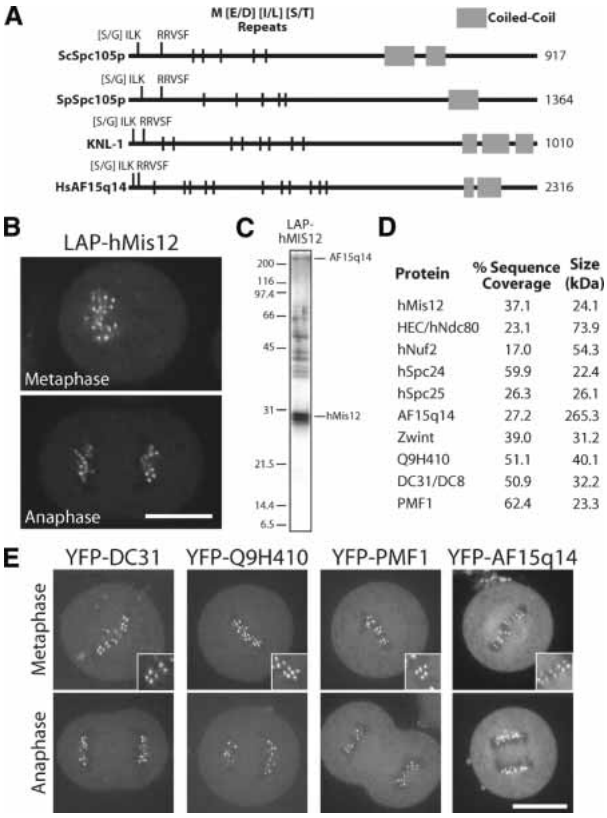

Figure 4. Human cells have a network of interacting proteins similar to that found using KNL-1 and KNL-3 purifications in *C. elegans*. (*A*) Similarity between KNL-1, fungal Spc105p, and human AF15q14. Schematic representation of *S. cerevisiae* Spc105p, *Schizosaccharomyces pombe* Spc105p, *C. elegans* KNL-1, and human AF15q14 proteins highlighting the invariant N-terminal [S/G]ILK and RRSVF motifs, the N-terminal MELT repeats, and the C-terminal coiled-coil domain. Position in the protein sequence is shown as a percentage of total length. AF15q14 was identified using a seedtop search (NCBI) of the nonredundant database using three degenerate MELT repeats as an input. There is 17.8% identity and 36.4% similarity between *S. pombe* Spc105p and human AF15q14, and 17.2% identity and 45.7% similarity between *C. elegans* KNL-1 and human AF15q14. (*B*) Localization of LAP–hMis12 to kinetochores in a stable clonal cell line derived from HeLa cells. Bar, 10 μm. (*C*) Purification of LAP–hMis12 from HeLa cells isolates multiple interacting proteins. Proteins were fractionated on a 13.5% polyacrylamide gel and visualized by silver staining. (*D*) Mass spectrometric analysis of the purification shown in *C* indicating the percent sequence coverage for each polypeptide with >5% coverage. A heat-shock protein and several forms of keratin present in the sample are not listed. (*E*) Imaging of T98G human tissue culture cells transiently expressing YFP fusions to the novel proteins identified in the hMis12 purification. Localization to punctate foci suggests that they localize to kinetochores during metaphase and anaphase. *Inset* shows blown-up image of paired dots representing sister kinetochores. Bars, 10 μm.

that are consistent with localization to kinetochores. These foci persisted into anaphase following separation of sister chromatids.

Thus, biochemical analysis in human cells defines a group of associated proteins with strong similarity to the proteins identified in *C. elegans* and confirms that KNL-1 defines a new widely conserved kinetochore protein family. Five of the KNL-1/3-interacting proteins are clearly conserved between *C. elegans* and humans, and it is possible that the remaining ones are orthologous proteins that have diverged in sequence.

Phenotypic analysis of the network of interacting proteins defines three functional classes

To functionally characterize the network of KNL-1/3-interacting proteins, we examined embryos depleted of each protein by RNAi. As described above, depletion of KNL-1 or KNL-3 results in a severe kinetochore-null (or KNL) phenotype (Fig. 1; Desai et al. 2003). In contrast, depletion of NDC-80 or Nuf2$^{\text{HIM-10}}$ results in a weaker NDC phenotype, in which chromosomes form a disorganized metaphase plate, show delayed sister chromatid separation, and exhibit extensive mis-segregation (Desai et al. 2003). To characterize the new proteins identified by our biochemical analysis, we first confirmed RNAi-mediated depletion of KBP-1, KBP-2, Spc25$^{\text{KBP-3}}$, and KBP-4 using immunofluorescence to monitor endogenous proteins (Fig. 3A). In the case of MIS-12, for which we do not have a suitable antibody, we demonstrated visible depletion of the LAP fusion protein using a dsRNA that targets both the endogenous gene and the fusion transgene (Supplementary Video 14).

Based on the similar loss-of-function phenotypes for Spc25, Ndc80, and Nuf2 reported in other systems (Janke et al. 2001; Wigge and Kilmartin 2001; Bharadwaj et al. 2004; McCleland et al. 2004), we expected that Spc25$^{\text{KBP-3}}$ depletion should result in an NDC phenotype. This was, indeed, the case, as can be seen in direct comparisons of embryos depleted of NDC-80 and Spc25$^{\text{KBP-3}}$ (Fig. 5A). The similarity of the depletion phenotypes extended to quantitative analysis of spindle elongation (Fig. 5B), which revealed similar premature separation of spindle poles.

Embryos depleted of MIS-12, KBP-1, or KBP-2 exhibited a distinct "MIS" phenotype (Fig. 5C; Supplementary Videos 6–8). In MIS embryos, metaphase plate formation was less perturbed than in NDC embryos, and the timing of chromosome separation was similar to that in wild-type embryos (data not shown). However, defects in chromosome alignment and segregation were frequently observed (Fig. 5C). MIS embryos have metaphase plates that are less compact and more disorganized than wild type. Although chromosome separation occurs in these embryos, sister chromatids are not clearly distinguishable during the first 10–20 sec (Fig. 5C, arrow). In addition, the separated chromatin masses are less coherent than wild type, with DNA frequently stretched along the spindle axis (Fig. 5C, arrowheads). Defects are also observed earlier during prometaphase, when chromosomes from maternal and paternal pronuclei persist in spatially distinct clusters significantly longer than in wild type (see Supplementary Videos 6–8). The placement of MIS-

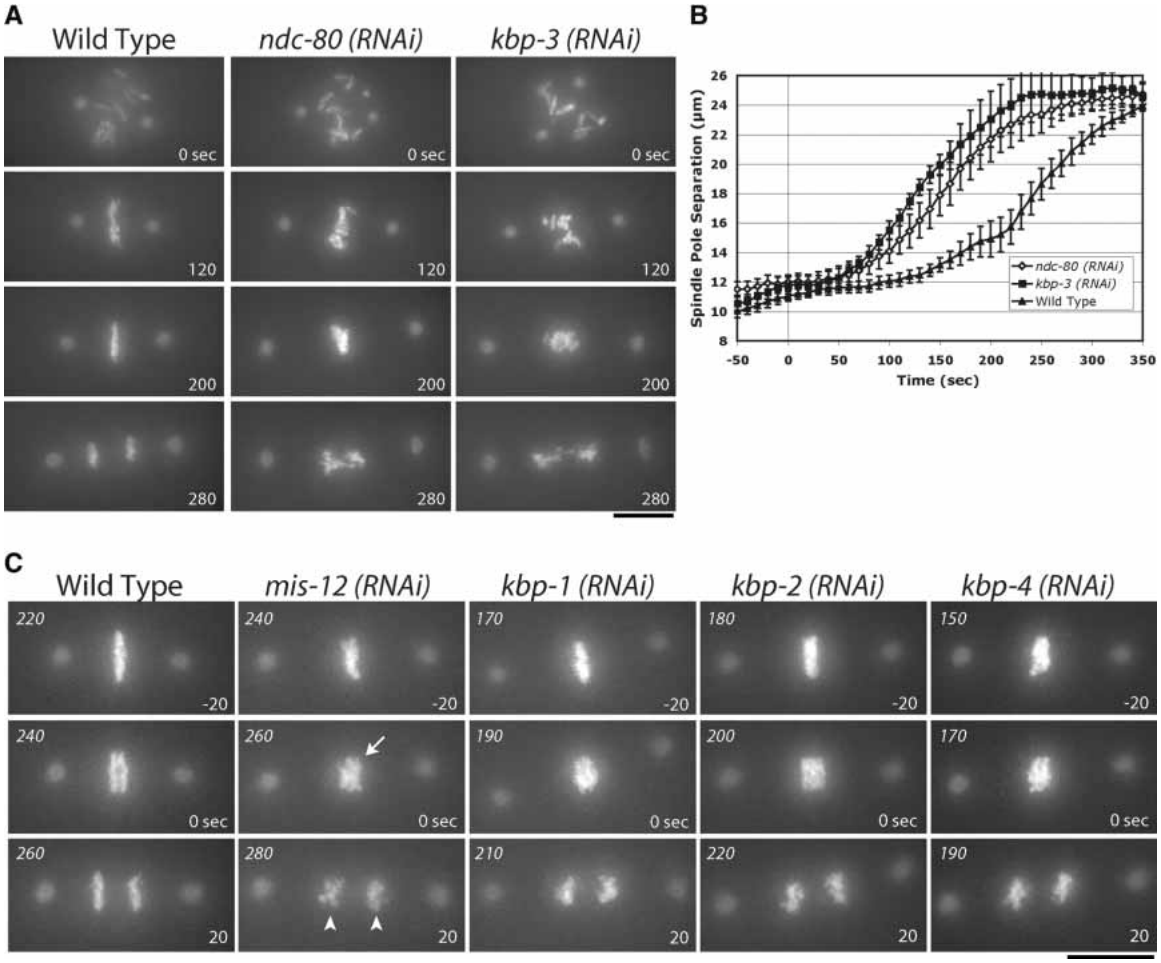

Figure 5. Depletion of KNL-1- and KNL-3-interacting proteins results in distinct chromosome segregation defects. (*A*) Spc25^{KBP-3} depletion results in a phenotype similar to depletion of NDC-80 and Nuf2^{HIM-10}. Still images from time-lapse movies of embryos expressing GFP–histone H2B and GFP–γ-tubulin of either wild-type embryos or embryos depleted of NDC-80 or Spc25^{KBP-3}. The times indicated are relative to NEBD. (*B*) NDC-80- and Spc25^{KBP-3}-depleted embryos exhibit similar premature spindle pole separation. The graph shows spindle pole separation kinetics in wild-type (n = 15), NDC-80-depleted (n = 12), and Spc25^{KBP-3}-depleted (n = 8) embryos. All sequences were time-aligned with respect to NEBD (0 sec), and the average spindle pole separation was calculated for each time point. Error bars represent the S.E.M. with a confidence interval of 0.95. (*C*) Depletion of MIS-12, KBP-1, KBP-2, and KBP-4 results in chromosome segregation defects. Still images from representative time-lapse movies are shown. The arrow indicates poor resolution of sister chromatids. The arrowheads indicate premature rounding of chromosome masses during anaphase. The numbers in italics on the *top left* of each panel are seconds after NEBD. The numbers on the *lower right* are time in seconds relative to visible chromosome separation. Bars, 10 μm.

12, KBP-1, and KBP-2 in a single phenotypic class is further supported by quantitative analysis of spindle elongation (see below).

KBP-4-depleted embryos also showed disorganized metaphase plates and lagging chromosomes (Fig. 5C), but in other assays KBP-4 behaves differently from MIS proteins (see below). The remaining protein, KBP-5, does not cause embryonic lethality when depleted, indicating that it is not essential for chromosome segregation. Thus, in vivo analysis of chromosome segregation defines three functionally distinct classes within the group of 10 interacting proteins: KNL (KNL-1, KNL-3), NDC (NDC-80, Nuf2^{HIM-10}, and Spc25^{KBP-3}), and MIS (MIS-12, KBP-1, and KBP-2).

MIS embryos exhibit a unique spindle 'bounce' phenotype

In addition to defects in chromosome alignment and segregation, a consistent and unique defect in spindle pole separation was observed in embryos depleted of MIS-12, KBP-1, or KBP-2. To visualize this defect, we generated kymographs from time-lapse sequences after spatially aligning the frames to place the spindle on the horizontal axis with the anterior spindle pole in a fixed position (Fig. 6A). This method helps visualize the kinetic profile for spindle pole separation (Fig. 6A, arrows) and its relationship to the onset of chromosome separation (Fig. 6A, arrowheads). Using this method on wild-type embryos,

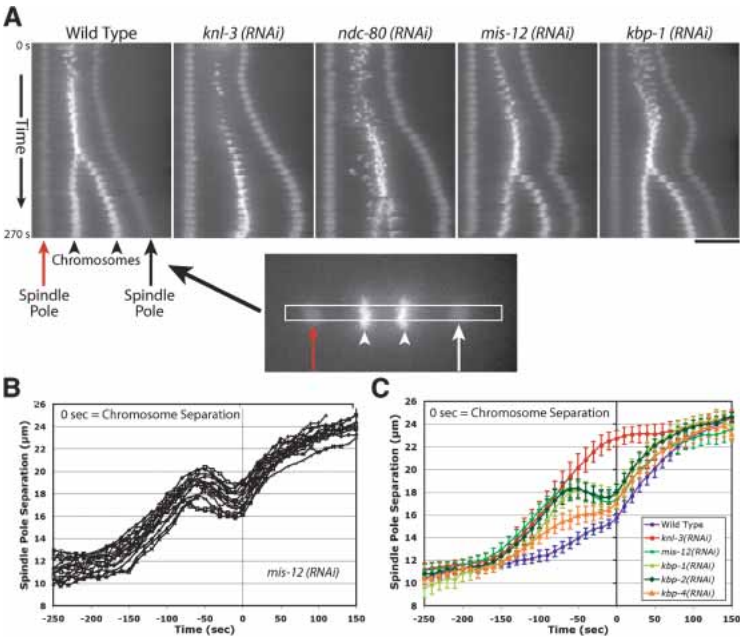

Figure 6. Depletion of MIS proteins results in a unique spindle "bounce" phenotype. (*A*) Still images from time-lapse movies of embryos expressing GFP–histone H2B and GFP–γ-tubulin were processed using an algorithm to fix the *X*–*Y* coordinate of one spindle pole (red arrow) throughout a movie and to rotate each frame such that the second spindle pole was at the same *Y*-coordinate. A 12-pixel-wide rectangular strip that included both spindle poles was cut from each frame and vertically montaged to generate a kymograph. The kymographs were initiated at NEBD, and the time interval between consecutive strips was 10 sec. In the kymographs, separation of both spindle poles (arrows) and the chromosomes (arrowheads) is visible. Bar, 10 μm. (*B*) Graph showing traces of spindle pole separation in 15 individual MIS-12-depleted embryos time aligned with respect to the onset of visible chromosome separation. (*C*) Graph plotting average spindle pole separation versus time for wild-type (n = 15), KNL-3-depleted (n = 18), MIS-12-depleted (n = 16), KBP-1-depleted (n = 11), KBP-2-depleted (n = 20), and KBP-4-depleted (n = 10) embryos aligned with respect to the onset of visible chromosome separation. The kinetic profiles for MIS-12-, KBP-1-, and KBP-2-depleted embryos are virtually indistinguishable. Because there is no chromosome separation in KNL-3-depleted embryos, the KNL-3 trace was aligned to maintain the same relationship with the wild-type trace shown in Figure 1. The average maximum elongation rates are 4.6 μm/min for *mis-12(RNAi)*; 5.7 μm/min for *kbp-1(RNAi)*; 5.0 μm/min for *kbp-2(RNAi)*; 5.4 μm/min for *knl-3(RNAi)*; 5.4 μm/min for *ndc-80(RNAi)*; and 2.5 μm/min for wild-type prometaphase spindle elongation. Error bars represent the S.E.M. with a confidence interval of 0.95.

the biphasic nature of spindle elongation, with an initial slow phase and a faster phase following anaphase onset, is clearly visible (Fig. 6A). The same method also illustrates the rapid and premature separation of spindle poles in KNL and NDC embryos (Fig. 6A). In contrast, in embryos depleted of MIS-12, KBP-1, or KBP-2 (Fig. 6A; data not shown), a spindle "bounce" phenotype was observed. Spindle poles separated rapidly after NEBD but always subsequently retracted, moving in toward the metaphase plate. Following chromosome separation, spindle pole separation occurred at wild-type rates.

To quantitatively analyze spindle pole separation in MIS embryos, we measured the distances between them at 10-sec intervals for 10–15 embryos per perturbation. Remarkably, when these data are aligned using the initiation of visible chromosome separation in each embryo, the kinetic profiles from different embryos almost perfectly overlap (Fig. 6B). In each case, the initial premature spindle elongation peaks ~60 sec prior to visible chromosome separation. Comparison of average spindle pole separation profiles for MIS-12-, KBP-1-, or KBP-2-depleted embryos, aligned using onset of chromosome separation (Fig. 6C), clearly indicates their similarity to each other and their difference from the KNL and NDC phenotypic classes (see Figs. 6C, 1A, 5B). KBP-4-depleted embryos also show a spindle elongation profile that is qualitatively similar to, but less severe than, MIS embryos (Fig. 6C).

Thus, the MIS phenotypic class is characterized by initial premature separation of spindle poles, similar in rate to KNL and NDC phenotypic classes (Fig. 6C). The rapid premature separation is followed by a recovery phase of ~60 sec during which there is a significant reduction in spindle length [1.57 ± 0.54 μm for *mis-12(RNAi)*, 0.83 ± 0.50 μm for *kbp-1(RNAi)*, and 1.13 ± 0.58 μm for *kbp-2(RNAi)*]. The qualitative and quantitative similarities between MIS-12-, KBP-1-, and KBP-2-depleted embryos strongly supports their placement in a common phenotypic class that is distinct from the KNL and NDC classes. The spindle pole separation profiles also suggest that, unlike the proteins in the KNL and NDC classes, the MIS proteins are not necessary to generate mechanically robust kinetochore–microtubule attachments, but are instead required for their timely formation.

Depletion of MIS proteins results in delayed and reduced outer kinetochore assembly

The unique spindle pole separation kinetics in embryos depleted of MIS proteins suggests that the ability of kinetochores to form mechanically robust microtubule attachments is initially defective but subsequently corrected. Given that cell cycle timing, assessed by measurcing the interval between NEBD and the onset of cytokinesis, is not significantly affected by depletion of MIS proteins (data not shown), it seemed unlikely that a cell-cycle-delay-based checkpoint accounted for the observed "bounce" in spindle elongation. Consistent with this expectation, simultaneous depletion of MIS-12 and Mad2^{MDF-2}, a component of the mitotic checkpoint (Kitagawa and Rose 1999), did not alter the kinetic profile of pole separation (data not shown).

To test whether kinetochore structure is disrupted in MIS embryos, we first analyzed the targeting of KNL-3.

We observed a severe reduction in KNL-3 at kinetochores in KBP-2-depleted embryos relative to similar-stage wild-type embryos (Fig. 7A). However, we also noticed that the amount of KNL-3 at kinetochores in the depleted embryos appeared variable. In particular, KNL-3 was more severely affected in earlier mitotic embryos relative to those with aligned chromosomes. Depletion of MIS-12 resulted in a similarly severe and variable affect on KNL-3 localization. Costaining of CENP-C^{HCP-4} and KNL-3 in *mis-12(RNAi)* embryos also indicated that, whereas the localization of KNL-3 was reduced, the localization of CENP-C^{HCP-4} and CENP-A^{HCP-3} was unaffected (Fig. 7B; data not shown).

To more directly examine the timing of KNL-3 localization, we depleted MIS proteins in embryos expressing GFP–KNL-3. GFP–KNL-3 is clearly visible on kinetochores prior to NEBD in control embryos (Fig. 7C; Supplemental Video 10). In contrast, in equivalently imaged *mis-12(RNAi)* (Supplementary Video 11) or *kbp-1(RNAi)* embryos (Fig. 7C; Supplementary Video 12), GFP–KNL-3 fluorescence was reduced throughout the embryo and no chromosomal localization was visible prior to NEBD. Whereas GFP–KNL-3 accumulated in the nuclear region following NEBD, it was not visible on the chromosomes until ~1 min prior to chromatid separation. Delayed and reduced kinetochore targeting of GFP–$Spc25^{KBP-3}$ was also observed following depletion of KBP-1 or MIS-12 (Fig. 7C; Supplementary Videos), indicating that NDC proteins were similarly affected.

Strikingly, the timing of visible recruitment of multiple kinetochore proteins in MIS embryos correlates with the onset of the inward spindle pole movement, suggesting that establishment of a functional kinetochore–microtubule interface is delayed following depletion of MIS proteins. Cumulatively, the spindle "bounce" phenotype and the delayed recruitment of multiple kinetochore proteins downstream from CENP-A^{HCP-3} and CENP-C^{HCP-4} indicate that the MIS proteins control the rate and extent of assembly of the outer regions of the kinetochore.

Pairwise depletion and targeting analysis place different functional classes into discrete positions in the kinetochore assembly hierarchy

Using pair-wise depletion/targeting analysis, we explored the molecular connectivity between the proteins characterized above during their assembly at kinetochores in vivo. This analysis complements the phenotype data to provide specific mechanistic interpretations for the different functional classes. Below, we summarize the results of this analysis for each functional class.

KNL: KNL-1 and KNL-3 act downstream from CENP-A^{HCP-3} and CENP-C^{HCP-4} and exhibit the most severe depletion phenotypes (Fig. 1). To determine the relationship between KNL-1 and KNL-3 during kinetochore assembly, we analyzed the localization of each in embryos depleted of the other protein. KNL-1 was completely delocalized in embryos depleted of KNL-3 (Fig. 8A). In contrast, KNL-3 persisted at kinetochores in KNL-1-depleted embryos, albeit at a reduced level relative to wild type (Fig. 8A,B; Supplementary Videos 10, 24). This observation suggests that KNL-3 functions upstream of KNL-1 in mitotic kinetochore assembly and predicts

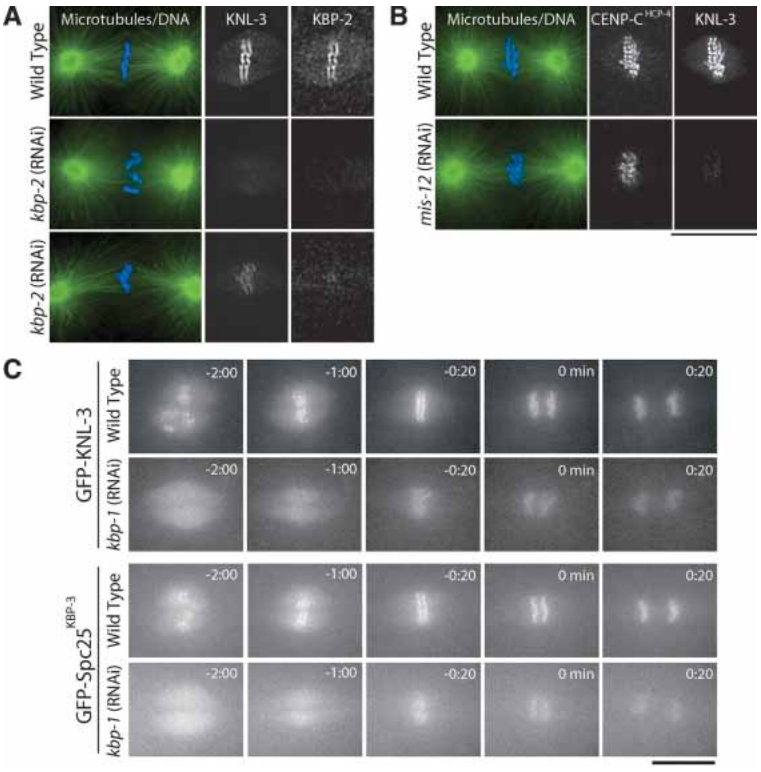

Figure 7. MIS proteins control the rate and extent of outer kinetochore assembly. (*A*) Depletion of KBP-2 results in a severe, but variable, defect in KNL-3 localization. Microtubules are shown in green and DNA in blue in the panels on the *left*. Two *kbp-2(RNAi)* embryos are shown to illustrate the variability in KNL-3 localization. In both, KNL-3 localization is significantly reduced relative to wild type. In the *bottom* embryo, more KNL-3 is detectable. All images were acquired and processed equivalently. (*B*) Depletion of MIS-12 reduces KNL-3 localization but does not affect CENP-C^{HCP-4}. Immunofluorescence images showing the localization of KNL-3 and CENP-C^{HCP-4} in wild-type and MIS-12-depleted embryos. (*C*) Live imaging indicates that depletion of MIS proteins causes a delay and reduction in kinetochore targeting of KNL-3 and $Spc25^{KBP-3}$. Selected images from time-lapse sequences of wild-type and KBP-1-depleted embryos expressing GFP–KNL-3 (*top* two rows) or GFP–$Spc25^{KBP-3}$ (*bottom* two rows). The times indicated are minutes prior to the onset of visible chromosome separation. Bars, 10 µm.

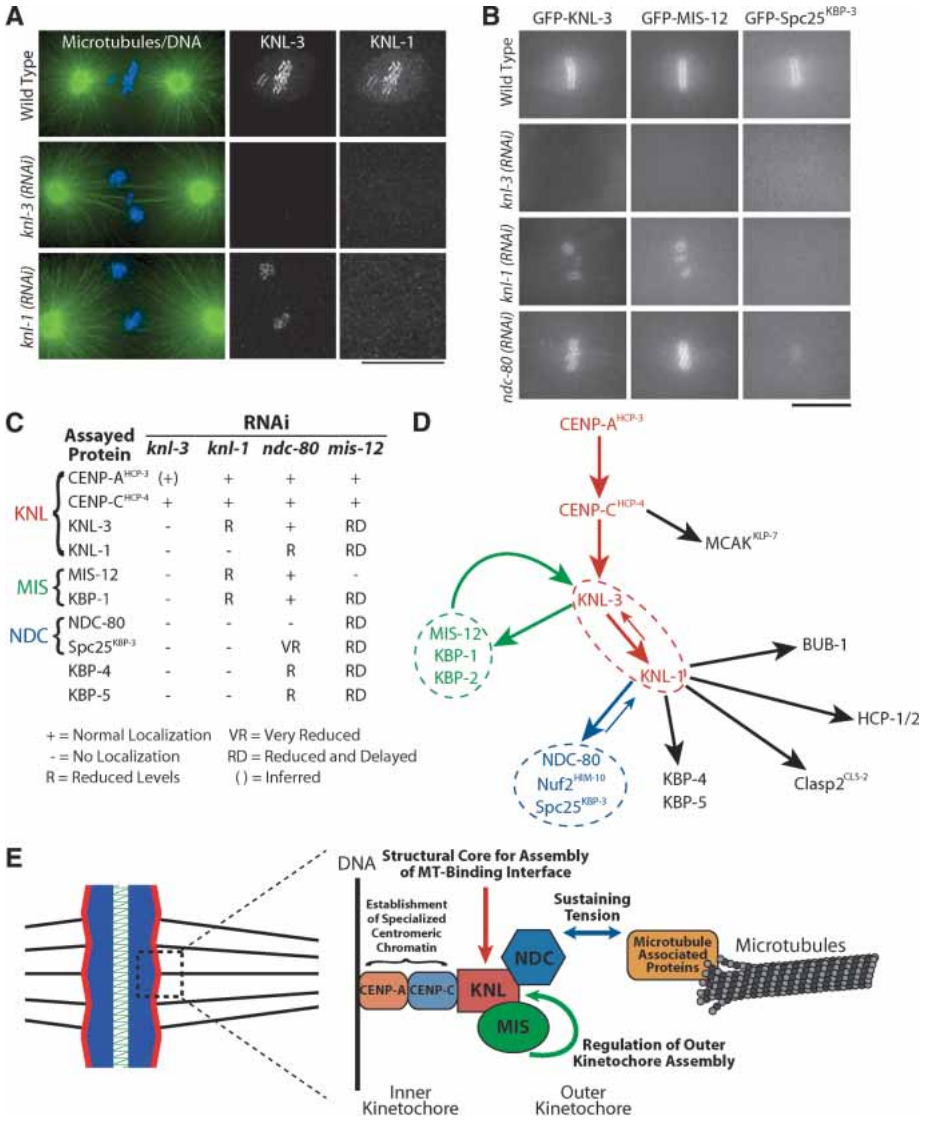

Figure 8. Placement of KNL, MIS, and NDC proteins in the molecular hierarchy of kinetochore assembly. (*A*) KNL-3 functions upstream of KNL-1. Immunofluorescence images showing the localization of KNL-3 and KNL-1 in wild-type, KNL-3-depleted, and KNL-1-depleted embryos. Microtubules are shown in green and DNA in blue in the panels on the *left*. Bar, 10 µm. (*B*) Still images from time-lapse sequences showing the localization of selected kinetochore markers (labeled on the *top* of each column) in embryos depleted of the indicated kinetochore components (labeled to the *left* of each row). Bar, 10 µm. (*C*) Summary of localization dependencies. Immunofluorescence using affinity-purified antibodies and live cell analysis of GFP fusions were used to examine localization dependencies as in *A* and *B*. Some data for KNL-1 and NDC-80 are from Desai et al. (2003). Five to 10 embryos were examined for each combination. (*D*) Diagram summarizing the targeting dependencies between *C. elegans* kinetochore proteins. (*E*) Summary model incorporating the dependency data summarized in *D* and the functions defined for the KNL, MIS, and NDC protein groups.

that proteins that require KNL-1 for their targeting should also require KNL-3. Consistent with our prediction, NDC-80 and HCP-1, which were shown previously to require KNL-1 for kinetochore targeting (Desai et al. 2003), also require KNL-3 (data not shown). In addition, localization of CENP-C^{HCP-4} and MCAK^{KLP-7} is unaffected in KNL-3-depleted embryos (Fig. 1D; data not shown), as is also true for KNL-1-depleted embryos (Desai et al. 2003). Extending this analysis to the other KNL-1/3-interacting proteins revealed that Spc25^{KBP-3}, KBP-4, and KBP-5 require KNL-3 as well as KNL-1 for their localization (Fig. 8A,B; Supplementary Videos). Thus, the KNL proteins are required to build the outer kinetochore.

MIS: Depletion of MIS proteins delays and reduces targeting of different kinetochore proteins downstream of CENP-A^{HCP-3} and CENP-C^{HCP-4} (Fig. 7). CENP-A^{HCP-3}, in turn, is required for targeting of MIS-12 (data not shown). Extending this analysis to KNL-1 and KNL-3 revealed that MIS-12 and KBP-1 require KNL-3, but not KNL-1, for their localization (Fig. 8B,C). This finding supports the placement of KNL-3 prior to KNL-1 during

kinetochore assembly and indicates that KNL-3 is required for the targeting of all of the KNL-1/3-interacting proteins.

NDC: Depletion of NDC-80 or Nuf2^{HIM-10} reduces, but does not eliminate, KNL-1 at kinetochores (Desai et al. 2003). In contrast, KNL-3 localization is unaffected by depletion of NDC-80 or Spc25^{KBP-3} (Fig. 8B; Supplementary Video 25), indicating that the NDC proteins function strictly downstream of KNL-3. MIS-12 and KBP-1 require KNL-3, but not KNL-1, for their localization. Thus, the normal targeting of MIS-12 and KBP-1 observed in *ndc-80(RNAi)* embryos (Fig. 8B; Supplementary Videos 28, 31) is in agreement with the expected result. Finally, localization of GFP–Spc25^{KBP-3} was severely reduced following NDC-80 depletion (Fig. 8B; Supplementary Video 40), consistent with work on homologous proteins in other systems (Janke et al. 2001; Wigge and Kilmartin 2001; Bharadwaj et al. 2004; McCleland et al. 2004). Thus, the NDC proteins function downstream of the KNL and MIS proteins during kinetochore assembly. The lack of a dramatic effect of the NDC proteins on kinetochore structure in combination with their requirement for resisting astral spindle forces (Fig. 5; Desai et al. 2003) suggests that they are necessary to sustain tension at the kinetochore–microtubule interface.

The results of the localization dependency analysis are summarized in Figure 8C. Figure 8D illustrates the assembly hierarchy based on these dependencies. The four kinetochore-null gene products form a linear hierarchy at the top of the mitotic kinetochore assembly pathway, whereas the MIS and NDC functional classes represent distinct branches. The observed phenotypes in combination with the dependency data suggest that KNL proteins represent a structural core required to generate the microtubule-binding interface, MIS proteins control the rate and extent of kinetochore assembly downstream of CENP-A^{HCP-3} and CENP-C^{HCP-4}, likely by regulating KNL-3 assembly, and the NDC proteins are required to sustain tension generated by bipolar kinetochore–microtubule attachments (Fig. 8E).

Discussion

During mitosis, the kinetochore forms a dynamic chromosomal attachment site for spindle microtubules. To study the molecular mechanisms underlying the interactions between kinetochores and spindle microtubules, we are using a combined functional and biochemical approach in *C. elegans*. Here, we identified a network of 10 associated kinetochore proteins that includes the kinetochore-null proteins KNL-1 and KNL-3, *C. elegans* homologs of Mis12 and the Ndc80 complex, widely conserved proteins that have been implicated in kinetochore function in other organisms, as well as four novel proteins. Using functional analysis of embryos depleted of each protein, we demonstrate that this network plays a central role at the interface with spindle microtubules. Parallel analysis of kinetochore function and assembly further leads us to conclude that three protein groups in this network contribute in different ways to coordinately generate a functional kinetochore–microtubule interface.

The distinct phenotypes observed in our functional analysis are unlikely to be derived from differences in protein depletion levels. In *C. elegans* embryos, RNAi-mediated depletion does not require intrinsic protein turnover because continued embryo production following injection of dsRNAs removes pre-existing protein. Quantitative Western blotting and immunofluorescence has shown that the RNAi conditions used here result in >90% depletion of a variety of proteins prior to the first mitotic division, including three proteins in the KNL-1/3 network (Hannak et al. 2001, 2002; Desai et al. 2003). Immunofluorescence on fixed embryos confirmed that the five new proteins analyzed here were depleted to a similar level (Figs. 1D, 4A). Three additional observations indirectly support the argument against variability in depletion levels as being the source of the phenotypic differences. First, depletion of different proteins within each functional class results in highly reproducible, quantitatively identical defects (see Figs. 1, 5, 6). In contrast, partial depletions typically result in more variable phenotypes (e.g., see Kirkham et al. 2003). Second, the phenotypic classification correlates with independent analysis of dependency relationships during kinetochore assembly. For example, all three NDC proteins require KNL-1 to localize to kinetochores, whereas both tested MIS proteins require KNL-3, but not KNL-1, for their targeting. Finally, simultaneous depletion of two proteins from the same group does not result in an enhanced phenotype as might be expected if depletions were partial. Specifically, double depletion of the NDC proteins NDC-80 and Nuf2^{HIM-10} or the MIS proteins MIS-12 and KBP-1 does not result in enhanced chromosome segregation defects (Desai et al. 2003; our unpublished results).

KNL-1 and KNL-3 form the core of the kinetochore–spindle microtubule interface

More than 25 worm kinetochore proteins have been identified thus far, yet depletion of only four results in the severe kinetochore-null phenotype. Two of these, KNL-1 and KNL-3, are part of the network of associated proteins analyzed here. Importantly, KNL-1 defines a new conserved kinetochore protein family. We demonstrate that AF15q14, the human homolog of KNL-1, interacts with hMis12 and subunits of the human Ndc80 complex and localizes to kinetochores throughout mitosis. AF15q14 is highly expressed in testis, cancer cells, and undifferentiated tumors, consistent with a role in cell proliferation (Takimoto et al. 2002). Based on the crucial role that KNL-1 and KNL-3 play at the kinetochore–microtubule interface, we expect that one of the other three novel human kinetochore proteins we have identified will be orthologous to KNL-3. KNL-1 and KNL-3 coimmunoprecipitate with CENP-C^{HCP-4}, suggesting a direct connection between these proteins and the chromatin at the base of the kinetochore. In total, our data suggest that KNL-3 interacts with the special-

ized centromeric chromatin structure established by CENP-A^{HCP-3} and CENP-C^{HCP-4} and, together with KNL-1, forms the core of the outer domains of the kinetochore that binds to spindle microtubules.

MIS proteins regulates the rate and extent of outer kinetochore assembly

Despite identification of Mis12 in a variety of species, its contribution to kinetochore function has remained unclear. Inactivation of Mis12 in yeast and humans results in aberrant chromosome segregation (Goshima and Yanagida 2000; Goshima et al. 2003). Similarly, chromosome segregation in *C. elegans* embryos depleted of MIS-12, or the functionally equivalent MIS proteins KBP-1 and KBP-2, is abnormal. In addition, spindle poles initially separate rapidly in MIS class embryos at rates identical to those in KNL embryos, indicating a failure to form stable bipolar microtubule attachments. However, this rapid separation is subsequently reversed, suggesting that MIS proteins are not strictly required to form kinetochore–microtubule attachments, but instead regulate the rate at which they form. Consistent with this idea, work on budding yeast Mis12^{Mtw1p} and the Mtw1 complex subunit Nsl1p, has suggested they are not required to maintain kinetochore–microtubule attachments after they are formed (Pinsky et al. 2003; Scharfenberger et al. 2003).

In embryos depleted of MIS-12 or KBP-1, the localization of proteins downstream from CENP-C^{HCP-4} to kinetochores is delayed. Strikingly, the appearance of detectable KNL-3 at kinetochores in these embryos coincides with the onset of inward pole movement. Because all of the outer kinetochore proteins that we tested require KNL-3 to target to kinetochores, the MIS proteins likely function by specifically controlling KNL-3 stability and/or localization, which in turn dictates the rate and extent of outer kinetochore assembly.

NDC proteins are required to sustain tension at the kinetochore–microtubule interface

NDC80 and its associated proteins play an essential role in chromosome segregation in all eukaryotes examined (Howe et al. 2001; Janke et al. 2001; Wigge and Kilmartin 2001; DeLuca et al. 2002; Desai et al. 2003; McCleland et al. 2003). The formation of an aberrant metaphase plate in *C. elegans* embryos depleted of NDC proteins suggests the presence of some kinetochore–microtubule interactions. However, spindle poles prematurely separate in NDC embryos with kinetics similar to KNL embryos, indicating that the attachments that occur are unable to resist astral pulling forces. Similarly in vertebrates, inhibition of Nuf2 or Ndc80/HEC prevents formation of stable kinetochore fibers, but the microtubule-dependent depletion of checkpoint proteins suggests the presence of kinetochore–microtubule interactions (DeLuca et al. 2003).

The phenotypic consequences of depleting NDC proteins can be explained by either (1) a direct role for these conserved proteins at the interface with spindle microtubules or (2) a general role in outer kinetochore assembly, because depletion of NDC-80 or Nuf2^{HIM-10} results in a reduction in kinetochore-localized KNL-1 and other KNL-1-dependent outer kinetochore components (Desai et al. 2003). Interestingly, a comparison of the MIS and NDC phenotypes helps clarify these possibilities. Depletion of MIS proteins leads to a reduction in the extent of recruitment of outer kinetochore components that is more severe than that resulting from depletion of NDC proteins, yet MIS embryos are still able to form tense bipolar attachments, whereas NDC embryos cannot. These results suggest that, in addition to a role in outer kinetochore structure, NDC components have a direct role at the microtubule interface. Based on the comparison between the three functional classes in the KNL-1/3 network, we propose that the widely conserved NDC proteins, although not required for kinetochore–microtubule attachments, are necessary to sustain tension at these attachments.

Identification of a conserved kinetochore architecture

Conservation of kinetochore components, despite divergence in the DNA sequences on which they assemble, is a well-established theme. However, poor sequence conservation of individual proteins suggests that this essential cellular machine is diverging rapidly. Therefore, it is important to determine whether there are conserved features of higher-order kinetochore structure. Our analysis demonstrates that conservation extends beyond primary sequence to physical interactions between groups of proteins and their requirements for kinetochore targeting. In *C. elegans*, the widely conserved kinetochore proteins MIS-12, NDC-80, and KNL-1 associate closely in the protein network defined here and additionally interact with CENP-C^{HCP-4}. Strikingly, similar associations exists in human cells, where hMis12, the human Ndc80 complex, and the KNL-1 homolog AF15q14 copurify from tissue culture cell extracts. These findings are supported by work in budding yeast, where physical associations between CENP-C^{Mif2p}, the four-subunit Mis12^{Mtw1p} complex, the four-subunit Ndc80 complex, and Spc105p have been observed (De Wulf et al. 2003; Nekrasov et al. 2003; Westermann et al. 2003). These similarities indicate that the network of interacting proteins identified here represents a core conserved element of kinetochore architecture in eukaryotes, despite dramatic sequence divergence of individual components. More significantly, the specific functions proposed here for the KNL, MIS, and NDC functional classes are likely to be broadly relevant.

Materials and methods

Worm strains and human tissue culture cells

For worm GFP or LAP fusions, the complete genomic region of a gene was cloned into pAZ132 (*unc-119*; pie-1 promoter driving

N-terminal GFP fusion) or pIC26 (*unc-119*; pie-1 promoter driving N-terminal GFP–TEV-S fusion) and integrated into DP38 (*unc-119 ed3*) using microparticle bombardment (Praitis et al. 2001) with a PDS-1000/He Biolistic Particle Delivery System (Bio-Rad). Worm strains are listed in Supplementary Table 1. For LAP–hMis12, hMis12 cDNA was cloned into pIC58 (YFP-TEV-S) and then subcloned into a Moloney murine leukemia retroviral plasmid (pBABEblast; Morgenstern and Land 1990; Shah et al. 2004). Stable cell lines derived from HeLa cells were generated as described previously (Shah et al. 2004). For transient expression of YFP proteins in T98G cells, pEYFP plasmids containing the full-length cDNA were transfected using Effectene (QIAGEN).

RNAi

L4 worms were injected with dsRNA (Supplementary Table 2) and incubated for 45–48 h at 20°C. The levels of each protein following depletion by RNAi were monitored using immunofluorescence (KNL-3, KBP-1, KBP-2, Spc25^{KBP-3}, and KBP-4) or imaging of stably expressed GFP fusion proteins (KNL-3, Spc25^{KBP-3}, MIS-12, KBP-1, KBP-4, and KBP-5). In each case, the target protein was depleted to the detection limit (>90%). KNL-1, NDC-80, and Nuf2^{HIM-10} have previously been shown to be effectively depleted using these conditions (Desai et al. 2003).

Microscopy

Images were acquired on a DeltaVision deconvolution microscope (Applied Precision) equipped with a CoolSnap CCD camera (Roper Scientific) at 20°C. For embryos expressing GFP–histone H2B and GFP–γ-tubulin, six z-sections were acquired at 2-μm steps using a 100×, 1.3 NA Olympus U-Planapo objective with 2 × 2 binning and a 480 × 480 pixel area at 10-sec intervals. Illumination was attenuated using 10% neutral density filter, and each exposure was 150 msec. For embryos expressing GFP–kinetochore proteins, six z-sections were acquired at 1-μm intervals using a 32% neutral density filter and 250-msec exposures. Z stacks were projected and imported into Metamorph (Universal Imaging) to rotate images, align spindle poles to generate kymographs, and for quantitative analysis of spindle pole elongation (see also Desai et al. 2003). Immunofluorescence was performed as described in Oegema et al. (2001) and Desai et al. (2003). Polyclonal antibodies against KNL-3 (residues 1–150), KBP-1, KBP-2, Spc25^{KBP-3}, and KBP-4 (full length) were generated as described previously (Desai et al. 2003). All images acquired using either a specific GFP-expressing strain or specific antibody were scaled identically.

Immunoprecipitations, LAP purifications, and mass spectrometry

N2 worms, or strains expressing LAP-tagged fusion proteins, were synchronized by bleaching and grown in liquid culture until each adult worm had ~10 embryos. For human purifications, tissue culture cells expressing LAP–hMis12 were grown in 15-cm dishes until ~70% confluent, and 100 ng/mL nocodazole was added for 14 h to enrich for mitotic cells. Worms or tissue culture cells were washed into lysis buffer (50 mM HEPES at pH 7.4, 1 mM EGTA, 1 mM $MgCl_2$, 100 mM KCl, 10% glycerol), drop-frozen in liquid N_2, and ground using a mortar and pestle. Immunoprecipitations were conducted on high-speed supernatant from adult worm or HeLa cell lysates essentially as described in Desai et al. (2003), except a total of 300 mM KCl and 0.05% NP-40 was added to the high-speed supernatant and wash buffers. Immunoprecipitated proteins were eluted from the antibody–Protein A resin using 50 mM Tris (pH 8.5), 8 M urea. For LAP purifications, the fusion proteins were isolated using anti-GFP antibodies as with the immunoprecipitations. TEV protease was then added to the bound proteins and incubated overnight at 4°C. The cleaved protein was then incubated with S protein agarose (Novagen) and eluted using 50 mM Tris (pH 8.5), 8 M urea. Mass spectrometry was conducted essentially as described in Cheeseman et al. (2001), except tandem mass spectra were searched against the most recent version of the predicted *C. elegans* proteins (Wormpep111) or the most recent database of predicted human proteins.

Acknowledgments

We are grateful to Paul Maddox for extensive discussions, assistance with microscopy, and the generation of the algorithms used to align images and measure spindle pole distances; John Kilmartin for pointing out the KNL-1/Spc105p homology; Tony Hyman for his support in the early stages of this work and for communicating unpublished information; Defne Yarar for extensive support and suggesting the human purifications; Jagesh Shah for help in generating the LAP–hMis12 cell line; Don Cleveland, Ben Black, Jagesh Shah, and Lars Jansen for critical reading of the manuscript; Tao Tao (NCBI) for assistance with the database search; and Yuji Kohara (National Institute of Genetics, Mishima, Japan) for gene-specific cDNAs. This work is supported by funding from the Ludwig Institute for Cancer Research to A.D. and K.O., and a grant from the National Center for Research Resources of the National Institutes of Health to Trisha Davis (PHS #P41 RR11823). I.M.C. is a Fellow of the Jane Coffin Childs Memorial Fund for Medical Research. K.O. is a Pew Scholar in the Biomedical Sciences. A.D. is a Damon Runyon Scholar supported by the Damon Runyon Cancer Research Foundation (DRS 38-04).

References

Bharadwaj, R., Qi, W., and Yu, H. 2004. Identification of two novel components of the human NDC80 kinetochore complex. *J. Biol. Chem.* **279:** 13076–13085.

Buchwitz, B.J., Ahmad, K., Moore, L.L., Roth, M.B., and Henikoff, S. 1999. A histone-H3-like protein in *C. elegans*. *Nature* **401:** 547–548.

Cheeseman, I.M. and Desai, A. 2004. Cell division: Feeling tense enough? *Nature* **428:** 32–33.

Cheeseman, I.M., Brew, C., Wolyniak, M., Desai, A., Anderson, S., Muster, N., Yates, J.R., Huffaker, T.C., Drubin, D.G., and Barnes, G. 2001. Implication of a novel multiprotein Dam1p complex in outer kinetochore function. *J. Cell Biol.* **155:** 1137–1146.

Cleveland, D.W., Mao, Y., and Sullivan, K.F. 2003. Centromeres and kinetochores: From epigenetics to mitotic checkpoint signaling. *Cell* **112:** 407–421.

DeLuca, J.G., Moree, B., Hickey, J.M., Kilmartin, J.V., and Salmon, E.D. 2002. hNuf2 inhibition blocks stable kinetochore–microtubule attachment and induces mitotic cell death in HeLa cells. *J. Cell Biol.* **159:** 549–555.

DeLuca, J.G., Howell, B.J., Canman, J.C., Hickey, J.M., Fang, G., and Salmon, E.D. 2003. Nuf2 and Hec1 are required for retention of the checkpoint proteins Mad1 and Mad2 to kinetochores. *Curr. Biol.* **13:** 2103–2109.

Desai, A., Rybina, S., Muller-Reichert, T., Shevchenko, A., Shevchenko, A., Hyman, A., and Oegema, K. 2003. KNL-1 directs assembly of the microtubule-binding interface of the kinetochore in *C. elegans*. *Genes & Dev.* **17:** 2421–2435.

De Wulf, P., McAinsh, A.D., and Sorger, P.K. 2003. Hierarchical

assembly of the budding yeast kinetochore from multiple subcomplexes. *Genes & Dev.* **17:** 2902–2921.
Goshima, G. and Yanagida, M. 2000. Establishing biorientation occurs with precocious separation of the sister kinetochores, but not the arms, in the early spindle of budding yeast. *Cell* **100:** 619–633.
Goshima, G., Kiyomitsu, T., Yoda, K., and Yanagida, M. 2003. Human centromere chromatin protein hMis12, essential for equal segregation, is independent of CENP-A loading pathway. *J. Cell Biol.* **160:** 25–39.
Grill, S.W., Gonczy, P., Stelzer, E.H., and Hyman, A.A. 2001. Polarity controls forces governing asymmetric spindle positioning in the *Caenorhabditis elegans* embryo. *Nature* **409:** 630–633.
Hannak, E., Kirkham, M., Hyman, A.A., and Oegema, K. 2001. Aurora-A kinase is required for centrosome maturation in *Caenorhabditis elegans*. *J. Cell Biol.* **155:** 1109–1116.
Hannak, E., Oegema, K., Kirkham, M., Gonczy, P., Habermann, B., and Hyman, A.A. 2002. The kinetically dominant assembly pathway for centrosomal asters in *Caenorhabditis elegans* is γ-tubulin dependent. *J. Cell Biol.* **157:** 591–602.
Howe, M., McDonald, K.L., Albertson, D.G., and Meyer, B.J. 2001. HIM-10 is required for kinetochore structure and function on *Caenorhabditis elegans* holocentric chromosomes. *J. Cell Biol.* **153:** 1227–1238.
Janke, C., Ortiz, J., Lechner, J., Shevchenko, A., Magiera, M.M., Schramm, C., and Schiebel, E. 2001. The budding yeast proteins Spc24p and Spc25p interact with Ndc80p and Nuf2p at the kinetochore and are important for kinetochore clustering and checkpoint control. *EMBO J.* **20:** 777–791.
Kirkham, M., Muller-Reichert, T., Oegema, K., Grill, S., and Hyman, A.A. 2003. SAS-4 is a *C. elegans* centriolar protein that controls centrosome size. *Cell* **112:** 575–587.
Kitagawa, R. and Rose, A.M. 1999. Components of the spindle-assembly checkpoint are essential in *Caenorhabditis elegans*. *Nat. Cell Biol.* **1:** 514–521.
Maddox, P.S., Oegema, K., Desai, A., and Cheeseman, I.M. 2004. 'Holo'er than thou: Chromosome segregation and kinetochore function in *C. elegans*. *Chromosome Res.* **12:** 641–653.
McCleland, M.L., Gardner, R.D., Kallio, M.J., Daum, J.R., Gorbsky, G.J., Burke, D.J., and Stukenberg, P.T. 2003. The highly conserved Ndc80 complex is required for kinetochore assembly, chromosome congression, and spindle checkpoint activity. *Genes & Dev.* **17:** 101–114.
McCleland, M.L., Kallio, M.J., Barrett-Wilt, G.A., Kestner, C.A., Shabanowitz, J., Hunt, D.F., Gorbsky, G.J., and Stukenberg, P.T. 2004. The vertebrate Ndc80 complex contains Spc24 and Spc25 homologs, which are required to establish and maintain kinetochore–microtubule attachment. *Curr. Biol.* **14:** 131–137.
Moore, L.L. and Roth, M.B. 2001. HCP-4, a CENP-C-like protein in *Caenorhabditis elegans*, is required for resolution of sister centromeres. *J. Cell Biol.* **153:** 1199–1208.
Morgenstern, J.P. and Land, H. 1990. Advanced mammalian gene transfer: High titre retroviral vectors with multiple drug selection markers and a complementary helper-free packaging cell line. *Nucleic Acids Res.* **18:** 3587–3596.
Nekrasov, V.S., Smith, M.A., Peak-Chew, S., and Kilmartin, J.V. 2003. Interactions between centromere complexes in *Saccharomyces cerevisiae*. *Mol. Biol. Cell* **14:** 4931–4946.
Nicklas, R.B. 1988. The forces that move chromosomes in mitosis. *Annu. Rev. Biophys. Biophys. Chem.* **17:** 431–449.
Oegema, K., Desai, A., Rybina, S., Kirkham, M., and Hyman, A.A. 2001. Functional analysis of kinetochore assembly in *Caenorhabditis elegans*. *J. Cell Biol.* **153:** 1209–1225.
Pinsky, B.A., Tatsutani, S.Y., Collins, K.A., and Biggins, S. 2003. An Mtw1 complex promotes kinetochore biorientation that is monitored by the Ipl1/Aurora protein kinase. *Dev. Cell* **5:** 735–745.
Praitis, V., Casey, E., Collar, D., and Austin, J. 2001. Creation of low-copy integrated transgenic lines in *Caenorhabditis elegans*. *Genetics* **157:** 1217–1226.
Rigaut, G., Shevchenko, A., Rutz, B., Wilm, M., Mann, M., and Séraphin, B. 1999. A generic protein purification method for protein complex characterization and proteome exploration. *Nat. Biotech.* **17:** 1030–1032.
Scharfenberger, M., Ortiz, J., Grau, N., Janke, C., Schiebel, E., and Lechner, J. 2003. Nsl1p is essential for the establishment of bipolarity and the localization of the Dam–Duo complex. *EMBO J.* **22:** 6584–6597.
Shah, J.V., Botvinick, E., Bonday, Z., Furnari, F., Berns, M., and Cleveland, D.W. 2004. Dynamics of centromere and kinetochore proteins; implications for checkpoint signaling and silencing. *Curr. Biol.* **14:** 942–952.
Starr, D.A., Saffery, R., Li, Z., Simpson, A.E., Choo, K.H., Yen, T.J., and Goldberg, M.L. 2000. HZwint-1, a novel human kinetochore component that interacts with HZW10. *J. Cell Sci.* **113:** 1939–1950.
Takimoto, M., Wei, G., Dosaka-Akita, H., Mao, P., Kondo, S., Sakuragi, N., Chiba, I., Miura, T., Itoh, N., Sasao, T., et al. 2002. Frequent expression of new cancer/testis gene D40/AF15q14 in lung cancers of smokers. *Br. J. Cancer* **86:** 1757–1762.
Westermann, S., Cheeseman, I.M., Anderson, S., Yates III, J.R., Drubin, D.G., and Barnes, G. 2003. Architecture of the budding yeast kinetochore reveals a conserved molecular core. *J. Cell Biol.* **163:** 215–222.
Wigge, P.A. and Kilmartin, J.V. 2001. The Ndc80p complex from *Saccharomyces cerevisiae* contains conserved centromere components and has a function in chromosome segregation. *J. Cell Biol.* **152:** 349–360.